Miranda-Valdez, Isaac Y.; Coffeng, Sebastian; Zhou, Yu; Viitanen, Leevi; Hu, Xiang; Jannuzzi, Luisa; Puisto, Antti; Kostiainen, Mauri A.; Mäkinen, Tero; Koivisto, Juha; Alava, Mikko J.

Foam-formed biocomposites based on cellulose products and lignin

Published in:
Cellulose

DOI:
10.1007/s10570-022-05041-3

Published: 01/03/2023

Document Version
Publisher's PDF, also known as Version of record

Cellulose (2023) 30:2253–2266
https://doi.org/10.1007/s10570-022-05041-3

ORIGINAL RESEARCH

Foam-formed biocomposites based on cellulose products and lignin

Isaac Y. Miranda-Valdez · Sebastian Coffeng · Yu Zhou · Leevi Viitanen · Xiang Hu · Luisa Jannuzzi · Antti Puisto · Mauri A. Kostiainen · Tero Mäkinen · Juha Koivisto · Mikko J. Alava

Received: 22 September 2022 / Accepted: 31 December 2022 / Published online: 9 January 2023

Abstract Foam-formed cellulose biocomposites are a promising technology for developing lightweight and sustainable packaging materials. In this work, we produce and characterize biocomposite foams based on methylcellulose (MC), cellulose fibers (CF), and lignin (LN). The results indicate that adding organosolv lignin to a foam prepared using MC and CF moderately increases Young's modulus, protects the foam from the growth of *Escherichia coli* bacteria, and improves the hydrophobicity of the foam surface. This article concludes that organosolv lignin enhances many properties of cellulose biocomposite foams that are required in applications such as insulation, packaging, and cushioning. The optimization of the foam composition offers research directions toward the upscaling of the material solution to the industrial scale.

Supplementary Information The online version contains supplementary material available at https://doi.org/10.1007/s10570-022-05041-3.

I. Y. Miranda-Valdez (✉) · S. Coffeng · L. Viitanen · X. Hu · L. Jannuzzi · T. Mäkinen · J. Koivisto · M. J. Alava
Department of Applied Physics, Aalto University, P.O. Box 11000, 00076 Aalto, Espoo, Finland
e-mail: isaac.mirandavaldez@aalto.fi

Y. Zhou · M. A. Kostiainen
Department of Bioproducts and Biosystems, Aalto University, P.O. Box 11000, 00076 Aalto, Espoo, Finland

A. Puisto
VTT Technical Research Centre of Finland Ltd, P.O. Box 1000, 02044 VTT, Espoo, Finland

Graphical abstract

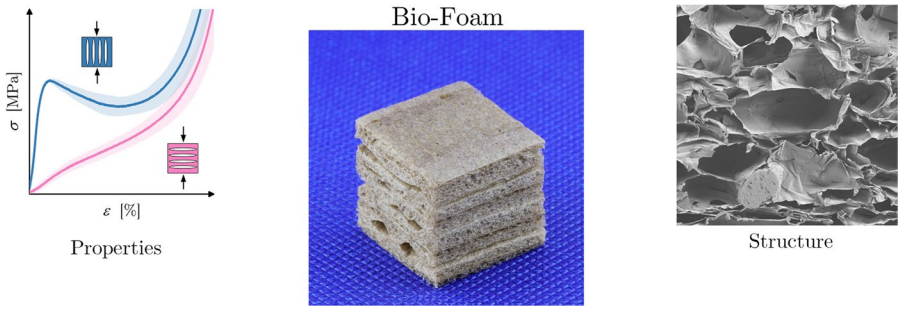

Keywords Cellulose · Lignin · Foam · Biomimicry · Biocomposite · Packaging

Introduction

Cellulose is the most prolific biopolymer on Earth, woody plants being a substantial and renewable source of it (Klemm et al. 2005). As a biopolymer, cellulose is biodegradable and exhibits remarkable mechanical properties (Gibson 2012). Today, due to advances in chemistry, cellulose can be processed in different morphologies, including foams, films, and aerogels, while maintaining its strength and biodegradability (Jiang and Ngai 2022). In this context, ongoing research on cellulose is increasingly taking advantage of cellulose miniaturization, dissolution, and derivatization for packaging fabrication (Reichler et al. 2021; Vuoriluoto et al. 2022). Cellulose, together with other biopolymers, is believed to be capable of substituting fossil-based polymers and alleviating the environmental pollution caused by plastic packaging (Li et al. 2021; Rhim et al. 2013).

Among the most important packaging products, foam cushioning and foam disposables (e.g., tableware) lack many sustainable alternatives to expanded and extruded polystyrene. Therefore, it is a common interest for the scientific community to innovate green alternatives that replace plastic foams (Cervin et al. 2016; Mort et al. 2021; Ottenhall et al. 2018). In response to this need, cellulose has been described as a flexible and affordable raw material for foam manufacture (Ferreira et al. 2021; Hjelt et al. 2021; Reichler et al. 2021). During the past decade, numerous articles have reported foam-like materials fabricated from cellulose pulp, nanocelluloses, and cellulose derivatives. These cellulose foams exhibit, for example, antimicrobial properties (Ottenhall et al. 2018), mechanical anisotropy (Reichler et al. 2021), thermal stability (Sehaqui et al. 2010), and hydrophobicity (Tejado et al. 2014). All of the aforementioned properties depend on the manufacturing process and the cellulose chemistry of the precursor.

In relation to cellulose, lignin is another biopolymer under increasing research due to its large availability as a byproduct of cellulose pulping (Balakshin et al. 2021). Biocomposites based on cellulose and lignin are an emerging research field, as they take inspiration from the biomimicking of the hierarchical structure of wood (Alam 2015). However, adding lignin to cellulose goes beyond the concept of biomimicry. As an additive, lignin can be used as a natural dye, rheology modifier, flocculant, antioxidant, bactericidal, strength modifier, and stabilizer during cellulose pyrolysis (Ma et al. 2021, 2015). For

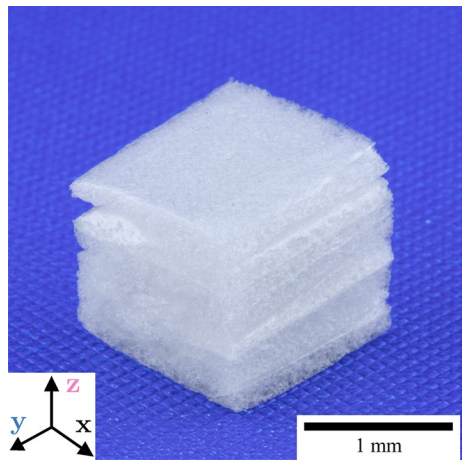

Fig. 1 Cellulose-based foam (Foam-MC) produced through the scalable process described by Reichler et al. (2021). The coordinate system indicates the directions in which the foam exhibits mechanical anisotropy, the y-axis being the strongest direction of the foam

example, Xu et al. (2022) produced a packaging biocomposite based on cellulose nanofibrils (CNF) containing lignin. According to the authors, the presence of lignin in CNF improved the stability and mechanical strength of the biocomposite (Xu et al. 2022). Similarly, a cellulose foam may benefit from the presence of lignin.

Previously, we reported on a scalable method for manufacturing biobased dry foams that mimic the cellular structure of wood (Reichler et al. 2021). Figure 1 shows our flagship cellulose foam. The approach we use to fabricate such lightweight structures features the combination of macroscopic cellulose fibers with a cellulose ether as a foaming agent. Our additive manufacturing produces foams with mechanical anisotropy (Reichler et al. 2021). We believe that incorporating lignin into the foam in Fig. 1 makes our material recyclable with cardboard. Furthermore, we hypothesize that lignin will enhance the rheology of the precursor wet foam as well as the mechanical performance. Consequently, the objective of this article is (I) to report for the first time a polymer foam based on cellulose and lignin produced with our technology, (II) to demonstrate the versatility of our foam manufacturing process, and (III) to evaluate the performance and structure of our biocomposite foams.

Materials and methods

To prepare the foams, we used food grade methylcellulose from Ashland Specialties Belgium. This cellulose ether has a degree of substitution of methyl groups close to 1.87 and an average molecular weight of 534 kDa. Bleached softwood kraft pulp (BSKP) obtained from CMPC pulp S.A. Santa Fe Mill and Pacífico Mill (Chile) was used as the reinforcement material. The fibers have an arithmetic mean length and width of 1.47 mm (ISO) and 30.41 µm, respectively (measurements performed with a Valmet Fiber Analyzer). The BSKP is obtained from *Pinus radiata* specimens, and the chemical composition of the pulp has been disclosed elsewhere (Andrade et al. 2021). In short, BSKP is composed of 85.5 wt.% cellulose, 13.6 wt.% hemicellulose, and less than 1 wt.% lignin (Andrade et al. 2021). The latter composition was confirmed with the technical datasheet handled by the provider, CMPC. Organosolv lignin obtained from wheat straw crops was used for sample preparation. We used tap water for all purposes to accommodate the industrial scalability of foam manufacturing. The quality of the water is reported in Miranda-Valdez et al. (2022). We prepared and characterized three different foams; Table 1 shows their formulations. We fixed the concentration of lignin to 0.5 wt.% since our preliminary research showed that concentrations lower than this do not significantly enhance the hydrophobicity of the foam surface. Also, we tested the effect of lignin on a methylcellulose/cellulose fiber foam since it is aimed by this article to observe the behavior when cellulose fibers and lignin are together in a foam.

Table 1 Percentage fractions of the weight of cellulose ether, cellulose fibers, lignin, and water comprising the wet precursors of the biocomposite foams prepared for this work

Sample	Cellulose ether (%)	Cellulose	Lignin	Water (%)
Foam-MC	1.5	0	0	98.5
Foam-CF	1.5	1.5%	0	97.0
Foam-LN	1.5	1.5%	0.5%	96.5

Foam manufacture

We fabricated the foams at our laboratory-scale facilities. First, for all samples, methylcellulose was dissolved in water at 50 °C. When the temperature of the aqueous methylcellulose suspensions reached 30 °C, we added the respective amounts of cellulose fibers, lignin, and water according to Table 1. The suspensions were vigorously stirred and cooled overnight at 3 °C. The foaming of the aforementioned suspensions proceeded through Hele-Shaw flow between two syringes plugged into each other. One syringe was filled with 30 ml of suspension, whereas the other was adjusted to leave a 30 ml free space. Then, the fluid is foamed by exchanging it between the syringes until the volume occupied by the foam reaches 60 ml. The dry foam is produced by printing rod-shaped wet foam structures parallel to each other until a foam sheet of 27 cm × 10 cm is formed. The printed wet foam is dried immediately using a heating lamp. A foam block is then produced by layering six foam sheets "glued" on top of each other. The gluing process involves gently spraying water on the foam sheets so that their surfaces bond together (samples are dried again). In a previous publication, we

provided more insights into the foam manufacturing process (Reichler et al. 2021). Finally, the density of the foam was measured by cutting cubic specimens of 15 mm per side. We calculated the foam density from the mass and volume of each cube, obtaining a standard deviation no larger than 2 kg/m^3.

Small amplitude oscillatory shear (SAOS)

Before foaming the suspensions, we inspected their rheological properties using SAOS temperature sweep tests. An MCR 302 rheometer (Anton Paar, Austria) equipped with Couette geometry deformed the suspensions at a constant angular frequency (ω) of 6.28 rad/s. Within a temperature (T) range from 15 to 70 °C (heat rate of 1 °C/min), a serrated bob tool (CP17/P6) dynamically applied a strain of 1%. Through SAOS tests, we identified the temperature at which the samples transitioned from viscoelastic liquids to viscoelastic solids. The viscoelastic transition temperature (T_v) is calculated from the experimental data of tan δ as a function of T, according to the slope intercept method reported by Miranda-Valdez et al. (2022). The loss factor is calculated on the basis of Eq. (1)

$$\tan\delta(\omega,T)=\frac{G''(\omega,T)}{G'(\omega,T)}, \tag{1}$$

where G'' and G' are the loss shear modulus and the storage shear modulus, respectively. Refer to Ghanbari et al. (2020) for more details about rheometry.

Optical microscopy

We inspect the foam surface with an optical microscope BX53M (Olympus, Japan) and a camera attachment DP74 (Olympus, Japan). Optical microscopy showed bubbles formed in the surface layers of the foams. We report photographs with a 20× objective.

Scanning electron microscopy (SEM)

We cut segments of different foam blocks, such as the one in Fig. 1, along the y-direction to observe the bubble structure of their cross-sections. To enhance electrical conductivity, we coated the samples with a thin layer of Au/Pd 80/20. In addition, the foam samples were mounted on carbon tape. The foams were inspected using a field emission scanning electron microscope (FE-SEM) from Zeiss Sigma VP (Germany). The electric potential remained constant (3 keV) and the images were generated from the SE2 signal.

Sessile drop goniometry

The wettability of the foam surfaces was examined by measuring the contact angle (*CA*) on a Theta Flex tensiometer (Biolin Scientific, Sweden). For the *CA* test, a 5 µl drop of water (resistivity of 18 MΩ cm) was deposited on the foam top surface parallel to the z-direction. The tensiometer analyzed with a camera the contact angle between the water drop and the surface; a $CA > 90°$ is typical of hydrophobic surfaces. The initial *CA* was recorded after 1.8 s and the last after 20 s. Each measurement was made in triplicate, and the arithmetic mean is reported.

Fourier-transform infrared spectroscopy (FTIR)

Infrared spectra of the foams were scanned using a Spectrum TwoTM $LiTaO_3$ spectrometer (Perkin Elmer, United Kingdom) equipped with an Attenuated Total Reflection accessory (Specac Quest, United Kingdom). Spectra were acquired at 25 °C in a wavenumber range of 4000–500 cm^{-1} with a resolution of 4 cm^{-1} after 30 scans. We identified the functional groups of cellulose, methylcellulose, and lignin from the spectra. The spectra did not require a baseline correction; however, the spectral intensity was normalized to the absorption intensity at 1056 cm^{-1}. The experiments were replicated three times, and no significant variation in the absorption bands was observed.

Thermogravimmetric analysis (TGA)

We surveyed the thermal decomposition of the foams using a Jupiter STA 449 F3 thermogravimetric analyzer (Netzsch, Germany). The studies were carried out under a protective He gas flow (70 ml/min) while heating from 50 to 700 °C at 10 °C/min. The STA analyzer measured the percentage of mass loss during the heating stage. All experiments were duplicated, and no significant differences were observed in the thermograms. The derivative of the mass loss

with respect to the temperature was calculated from the experimental results.

Uniaxial compression tests

To measure the elastic properties and deformation of the foams, we compressed samples (geometry of ≈ 1.5 cm per side), such as the one shown in Fig. 1. Compression tests were performed on an Electroplus® E1000 dynamic testing machine (Instron, United Kingdom). The protocol consisted of compressing five specimens of each sample in the y-direction (parallel to the foam rod-like structure) and in the z-direction (perpendicular to the rod-like structure) at a deformation rate of 30 mm/min. We plotted the stress (σ) *vs.* strain (ε) curves using the average and standard deviation obtained from five measurements.

The elastic modulus was calculated by finding the maximum slope of the elastic part of the stress-strain curve and fitting a slope in a range of 20% ε before this point. The slope of the fitted line corresponds to the Young's modulus (E) of the material. The yield point is defined as when the stress diverges 10% from the fitted line. See Fig. S1 to Fig. S3 for visualizing the fitting process and the determination of the yield points. Lastly, the area under the stress-strain curve (integrated from 0 to 70% ε) was used to estimate energy absorption (W).

Antimicrobial testing

We evaluated the antibacterial and antifungal activity of the foams against *Escherichia coli* (*E. coli*) and *Saccharomyces cerevisiae* (yeast), respectively. All chemical reagents were analytical grade and were used without further purification. *E. coli* was cultivated in an LB broth (lysogeny) and yeast in a YPD broth (yeast extract peptone dextrose). Ultrapure water with a resistivity of 18 MΩ cm was used for all experiments. Briefly, the experiments proceeded as follows. The foams were first weighed and then sterilized with UV light for 20 min. Meanwhile, the overnight cell culture prepared was diluted into a suspension of 106 CFU/ml (CFU stands for colony formation unit). Subsequently, approximately 100 mg of foam materials were added to 20 ml of diluted suspension for overnight incubation. The incubation temperature for *E. coli* and yeast were 37 °C and 30 °C, separately. The difference in optical density (*OD*) of cell suspensions at 600 nm was measured with an eppendorf BioPhotometer plus spectrometer. The results after incubation time were compared with a control cell culture and reported using Eq. (2). All materials were tested in triplicate. The error bars show the standard deviation.

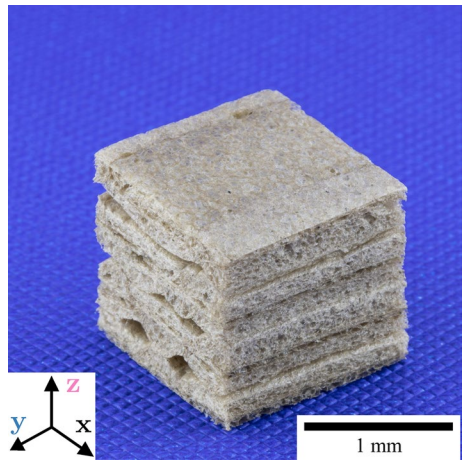

Fig. 2 Cellulose-based foam containing lignin (Foam-LN). Foam is produced through the scalable process described by Reichler et al. (2021). The coordinate system indicates the directions on which the foam exhibits mechanical anisotropy, the y-axis being the strongest direction of the foam

Table 2 Mechanical properties of biocomposite foams

Sample	T_v (°C)	E_y (MPa)	ε_y (%)	E_z (MPa)	ρ (kg/m^3)	E_y/ρ	E_z/ρ	W_y (kJ/m^3)	W_z (kJ/m^3)
Foam-MC	48.4	0.37 ± 0.005	6.58	0.047 ± 0.003	18.8	0.019	0.002	17.8	10.5
Foam-CF	40.6	1.39 ± 0.010	4.35	0.089 ± 0.004	31.1	0.035	0.002	35.6	19.2
Foam-LN	39.2	2.18 ± 0.015	4.80	0.106 ± 0.003	44.9	0.049	0.002	62.0	28.0

The results of T_v were estimated using the slope intercept method reported by Miranda-Valdez et al. (2022). E_y stands for the elastic modulus in the y-direction and E_z in the z-direction. ε_y represents the yield strain in the y-direction

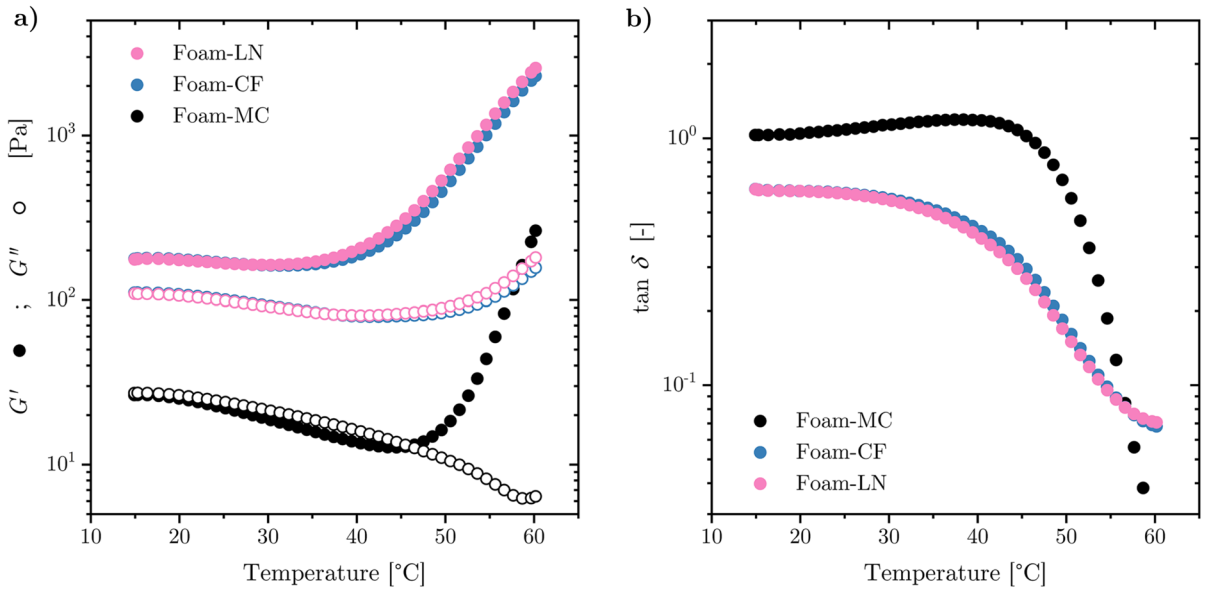

Fig. 3 SAOS temperature sweep results obtained for the precursor foam suspensions. The experimental conditions were an angular frequency of 6.28 rad/s and a heating rate of 1 °C/min. **a** Storage and loss modulus as a function of temperature, and **b** loss factor (tan δ) as a function of temperature

$$\Delta OD = \frac{OD_{control} - OD_{sample}}{OD_{control}} \cdot 100\% \quad (2)$$

Results and discussion

Foam manufacture was based on the lower critical solution temperature (LCST) of methylcellulose, which was responsible for T_v identified in Table 2. Above this transition temperature, the precursor foam suspensions became more elastic than viscous. Therefore, our additive manufacturing took advantage of the latter phenomenon by heating the printed wet foam rods above their T_v. After drying, the rods were assembled in different geometries, allowing us to fabricate anisotropic biobased foams such as the ones depicted in Figs. 1 and 2. We included a coordinate system next to the foams in Figs. 1 and 2 to illustrate their anisotropy. The coordinate system indicates the directions on which the foams can exhibit distinct mechanical properties, the directions y- and z- being the subject of discussion in this article.

Henceforth, as Table 1 displayed, we refer to the foam sample containing only methylcellulose (MC) as Foam-MC. The foam sample composed of MC and cellulose fibers (CF) is labeled Foam-CF, and Foam-LN indicates the sample prepared using MC, CF, and lignin (LN).

Rheological behavior

For foam fabrication, it is relevant to evaluate the T_v and elasticity of any precursor suspension, as these characteristics rule out the feasibility of printing and drying. SAOS experiments allowed us to characterize the elasticity of suspensions by measuring G'. Furthermore, T_v was estimated from the change in energy dissipation (tan δ). Figure 3a shows the former and Fig. 3b the latter. Consequently, the SAOS results for all suspensions demonstrated that, when heated, G' increased sharply (Fig. 3a), while tan δ changed oppositely (Fig. 3b). These changes in G' and tan δ are more noticeable when the suspensions were heated above T_v (Table 2). The viscoelastic behavior of G' and tan δ arises from the aqueous MC matrix of each suspension, which forms a fibril network (Coughlin et al. 2021; Lott et al. 2013). As the MC matrix forms a fibril network, a large number of non-covalent interactions appear between the hydrophobic sites of the polymer (Arvidson et al. 2013).

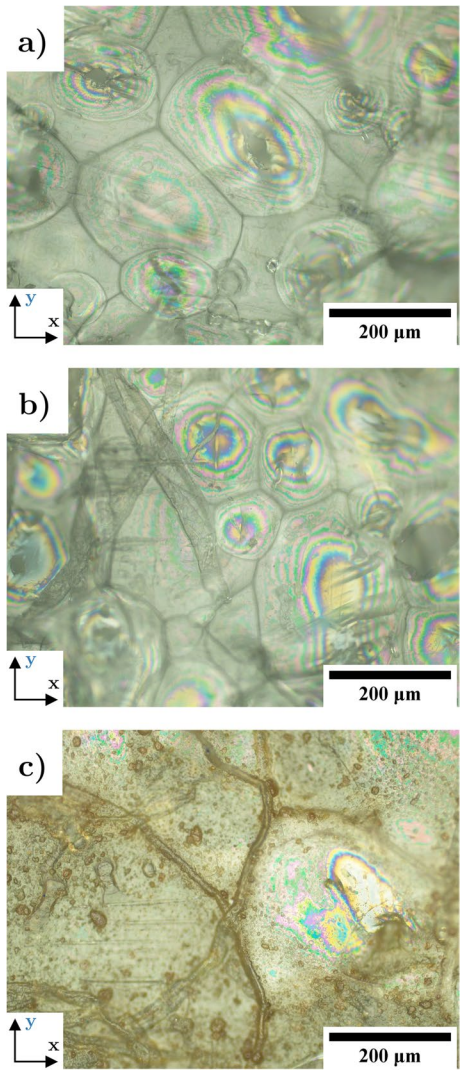

Fig. 4 Optical microscopy images of **a** Foam-MC, **b** Foam-CF, and **c** Foam-LN. The images show the surface of the biobased foams. Furthermore, the coordinate system indicates the direction in which the rod-shaped structure is oriented

Regarding the rheological differences in the suspensions studied, Fig. 3a depicts that Foam-CF and Foam-LN showed higher G' than Foam-MC. This effect was expected because the solid content in Foam-CF and Foam-LN is higher than in Foam-MC. Furthermore, G' of Foam-CF and Foam-LN show similarities in shape and magnitude, implying that mechanical reinforcement in suspensions is primarily due to the incorporation of CF. The results reported by multiple authors indicate that the total solid content in a system containing a gel-forming material,

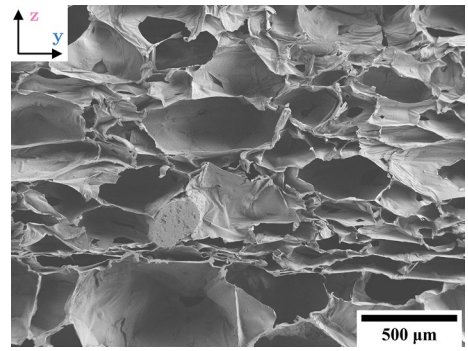

Fig. 5 Scanning electron microscopy image of the cross-section of Foam-LN. The elongation of the bubbles orients toward the y-direction of the foam

such as MC, increases G' and reduces T_v of the systems. For example, Miranda-Valdez et al. (2022) modeled the decrease in T_v as a function of the CF content in an MC suspension. Similarly, Korhonen and Budtova (2019) studied the CF content and its impact on the gelation time of dissolving pulps.

In our case, we observed a decreasing T_v as a function of the solid content of the suspension, Foam-MC being the suspension with the lowest solid content and, therefore, the highest T_v (Table 2). Although the mechanism by which T_v decreases as a function of the content of CF or LN is uncertain, it is believed to occur due to the formation of hydrogen bonds between the fibers and the dissolved matrix (Budtova and Navard 2016; Korhonen and Budtova 2019; Miranda-Valdez et al. 2022). Understanding the gelation mechanism of MC in relation to the CF and LN content is beyond the scope of this article, but we acknowledge its importance. From the plot in Fig. 3b, we can only infer that the activation energy of the gelation process should decrease when CF and LN are added to the MC suspensions. This can be interpreted from the magnitude of energy dissipation ($\tan\delta$) presented by Foam-CF and Foam-LN, which is less than that of Foam-MC.

Morphological and structural characterization

The optical microscopy images in Fig. 4 show a bubble-like structure with defined boundaries in Foam-MC (Fig. 4a) and Foam-CF (Fig. 4b). However, this structure is less noticeable for Foam-LN (Fig. 4c). We attribute the disappearance of the bubble boundaries

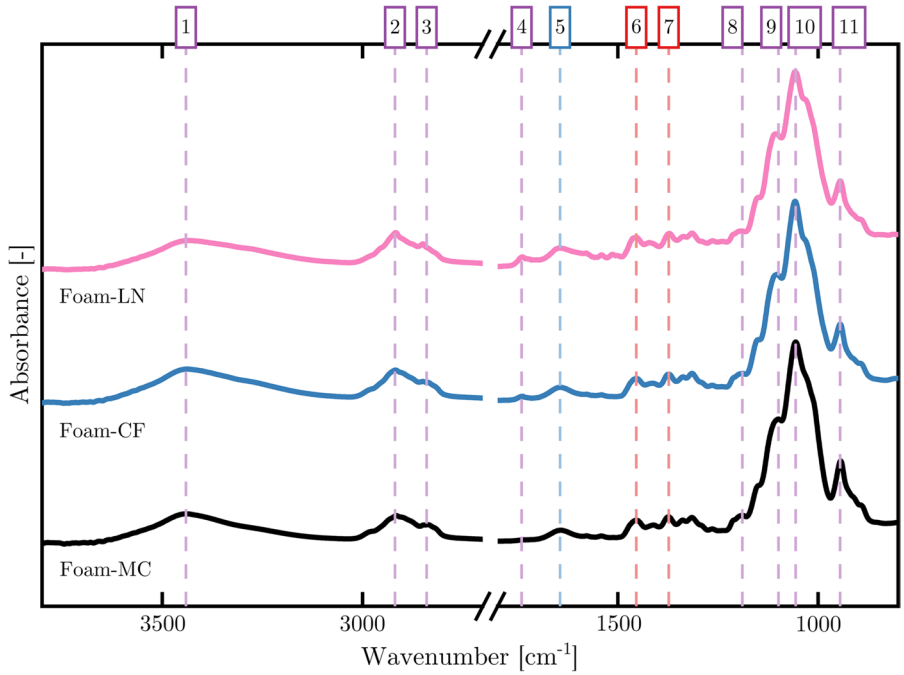

Fig. 6 Fourier-transform infrared spectra of the biobased foams; Foam-MC, Foam-CF, Foam-LN. The numbers assigned on the top axis correspond to the functional groups vibrations identified in Table 3

Table 3 The functional groups of cellulose identified from the absorption bands in the FTIR spectra of the biocomposite foams

Vibration	Foam-MC	Foam-CF	Foam-LN	Number
OH str.	3441	3436	3435	1
CH str.	2919	2918	2917	2
CH str.	2837	2840	2850	3
C=O str.	–	1740	1739	4
H_2O abs.	1644	1645	1646	5
CH_2 def.	1454	1454	1454	6
CH def.	1373	1373	1371	7
COC str.	1189	1188	1190	8
in-plane str. of ring	1099	1103	1105	9
CO str. at C6	1056	1057	1057	10
Ring in-phase	944	945	945	11

Larkin (2018) was taken as a reference for the assignment of the bands. The abbreviation str. stands for stretching, def. for deformation, and abs. for absorption

to a densification effect on the foam surface resulting from the addition of lignin to Foam-LN (see the density values in Table 2). Lignin, as a natural binder, can contribute to the formation of hydrogen bonds, improving the adhesion between all the constituents. Examples of these effects can be observed in biomass pellets, where lignin was shown to improve bridging and bonding after drying (Kaliyan and Morey 2010; Nanou et al. 2018). From SEM analysis in Fig. 5 and Fig. S4 to Fig. S6, we point out that Foam-MC, Foam-CF, and Foam-LN possess a closed cell structure with bubbles elongated over the y-direction (quasi-hexagonal prism structure).

In relation to the surfaces presented in Fig. 4, we also measured their wettability by testing the water *CA*. Foam-LN exhibited an initial water *CA* of 117° ± 4°, which remained above 90° even after 20 s. However, although Foam-MC and Foam-CF had an initial *CA* close to 90°, after 20 s their *CA* decayed to the hydrophilic range. Accordingly, lignin contributed to the production of a hydrophobic surface on Foam-LN. This hydrophobic effect may arise from a combination of surface lignin and surface roughness in Foam-LN (Ferreira et al. 2020; Yang et al. 2006). Looking at Fig. 4a, b, the surfaces of Foam-MC and Foam-CF are smooth, while Foam-LN has many textures. Pictures of the droplet *CA* on the foam surface are provided in Fig. S7 to Fig. S9. Lignin in the Foam-LN system may be driven to the surface (liquid-gas interface) as a result of enthalpic changes, which may involve reordering hydrogen bonds during the foam-forming process (Chandler 2005). However,

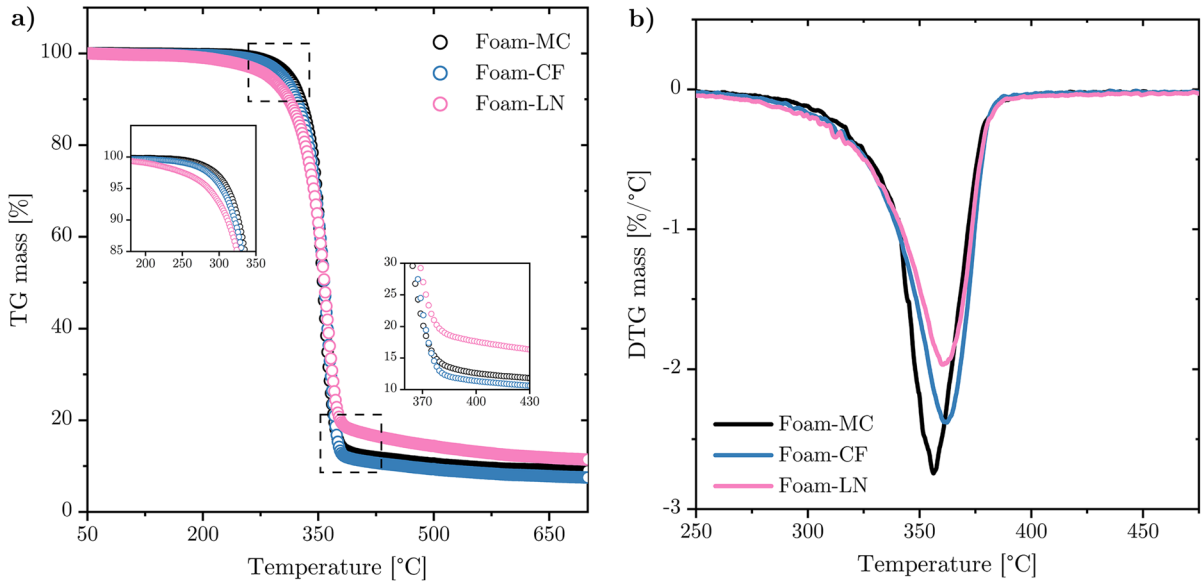

Fig. 7 Thermogravimmetry experiments showing **a** the mass loss as a percentage of the biobased foams and **b** the derivative of the mass loss with respect to the temperature. The minimum in DTG is related to the maximum mass loss rate of the biobased foams

understanding the hydrophobic behavior of Foam-LN requires more studies.

Regarding the chemical structure of the foams, from the FTIR spectra in Fig. 6, we identified the spectral position of the relevant functional groups of cellulose. Table 3 collects the information mentioned above. At 3435–3441 cm^{-1}, the OH stretching vibration appears for all foams. Compared to Foam-MC and Foam-CF, it is possible to visualize the effect of lignin on Foam-LN on the stretching vibration of the

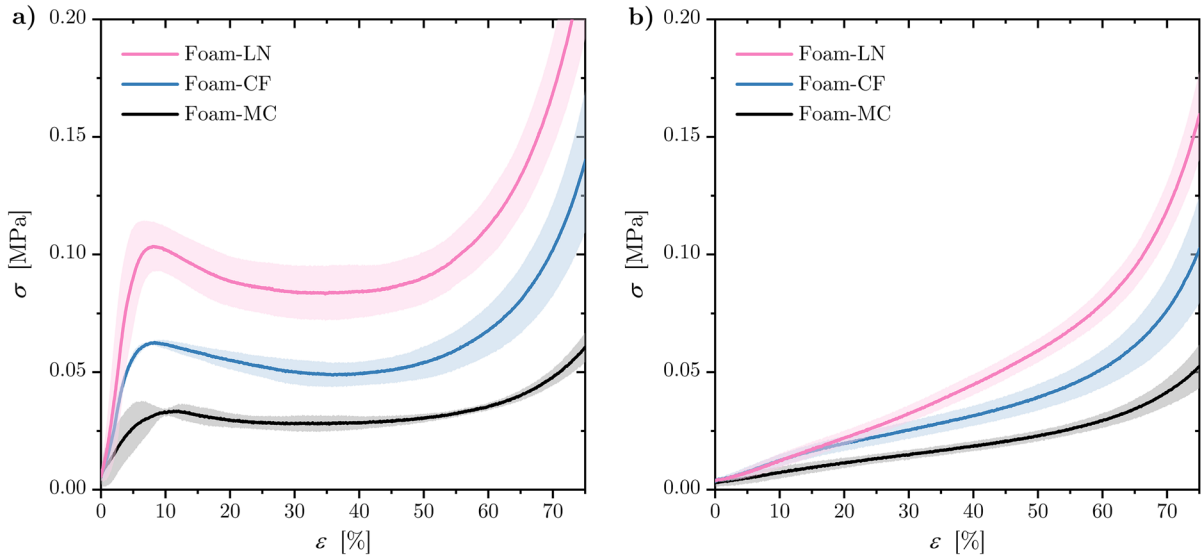

Fig. 8 Compression tests were performed on the biobased foams. The results show the classical engineering stress/strain curve obtained after compressing the foam specimens in **a** the y-direction and **b** the z-direction. The difference in mechanical behavior demonstrates the anisotropy of the foams

CH groups, since the wavenumber is displaced from 2840 to 2850 cm^{-1}. This displacement results from CH located in aromatic methoxyl groups and methyl groups of the lignin side chains (Boeriu et al. 2004). Basically, all foams showed identical FTIR spectra; nevertheless, for Foam-CF and Foam-LN, an absorption band appears at 1740 cm^{-1}. This band is in the carbonyl region and may be related to residual lignin in the BSKP constituting Foam-CF and the organosolv lignin added to Foam-LN. At spectral positions close to 1740 cm^{-1}, lignin typically exhibits the C = O stretching of unconjugated ketones and carbonyl groups (Boeriu et al. 2004; Derkacheva and Sukhov 2008; Faix 1991).

As the final part of the structural characterization, in Fig. 7, we evaluated the thermal decomposition of the foams. Interestingly, the foam mass was stable at temperatures close to 200 °C. However, the addition of CF and LN accelerated the onset of the decomposition reaction. This can be observed in the zoom-in graph in Fig. 7a for the 225–350 °C range and can be attributed on a part to the hemicellulose content present in CF, which decomposes at lower temperatures than cellulose (Yang et al. 2007; Yu et al. 2017). Regarding Foam-CF, adding cellulose fibers to the foam reduced the carbonization yield, compared to the yield observed for Foam-MC. Further studies are needed to determine the pyrolysis mechanism between MC and CF. In the case of Foam-LN, pure lignin is known to thermally decompose at lower onset temperatures than cellulose and in a wider temperature range (Ma et al. 2015; Trogen et al. 2021; Yang et al. 2007; Yu et al. 2017). In cellulose/lignin blends, Miranda-Valdez (2022) and Trogen et al. (2021) observed that lignin transfers its thermal behavior when mixed with cellulose. Regarding the offset of thermal decomposition (see zoom-in plot in Fig. 7a for 360–430 °C range) of Foam-LN, lignin promoted a higher mass yield. From Fig. 7b, the derivative of the mass shows that the maximum decomposition rate shifted to higher temperatures as CF and LN were added to the foam. Furthermore, the peak minimum shifts to higher temperatures for Foam-CF and Foam-LN. Foam with such thermal properties, such as Foam-LN, would be of particular interest for tailoring biocarbon sponges in the future.

Compression behavior

Figure 8a, b depict the foam compression results. The first collects the stress-strain curve obtained from compressing in the y-direction, and the second comes from testing in the z-direction. From Fig. 8, we calculated the mechanical properties, as explained in the methods section, and summarized them in Table 2. In general, the observed mechanical anisotropy in Fig. 8a, b comes from the rod-like structure of the foams assembled parallel to the y-direction and the open mold fabrication process (Gibson and Ashby 1997; Reichler et al. 2021). Furthermore, the closed cell geometry of the foams and the elongated bubbles, as shown in the SEM image of Fig. 5, align parallel to the y-direction, increasing the mechanical anisotropy of the foams (Gibson and Ashby 1997; Reichler et al. 2021).

The compression of the samples in the y-direction (Fig. 8a) showed the three typical deformation stages described by Ashby and Medalist (1983). Initially, (1) as the foams deformed, they showed an elastic region, (2) which is followed by a plateau of deformation (plastic yielding for plastic foams and elastic buckling for elastomeric foams). (3) After the plateau, the closed cell structure collapses, densifying the foams. According to Gibson and Ashby (1997), the stress-strain profile of the foams y-direction (Fig. 8a) would resemble a plastic foam, while the z-direction would for an elastomeric foam (Fig. 8b). For an elastomeric foam, the onset of stress typically begins with a lower strain than for a plastic foam (Gibson and Ashby 1997). The first is the case observed in Fig. S1 to Fig. S3, a fact supporting that the foams exhibit plastic and elastomeric behavior in the y- and z-direction, respectively (Gavin et al. 2018).

Concerning foam composition and its effect on compression behavior, we compare foam samples by referring to their stiffness index (Table 2). Using the stiffness index allows us to include the density effect in the assessment. First, compared to Foam-MC, the fibers in Foam-CF increased stiffness in the y-direction, but not in the z-direction. The stiffness index in the y-direction of Foam-CF follows the fiber-reinforcement principle since both the MC matrix and CF carry a certain proportion of the compressive load. For example, Kerche et al. (2021) reported that microfibrillated cellulose fibers increased the mechanical performance of a polyurethane foam.

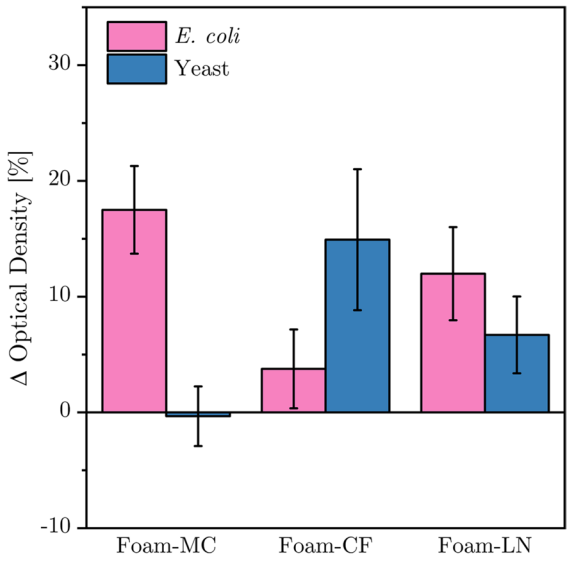

Fig. 9 Antibacterial and antifungal activity of biobased foams against *Escherichia coli* (*E. coli*) and *Saccharomyces cerevisiae* (yeast). A positive *ΔOD* indicates the susceptibility of biobased foams

However, the stiffness observed in Foam-CF and Foam-LN is related to the fiber orientation and length. Due to the fiber length (average 1.47 mm), CF can only align parallel to the y-direction, making it unsuitable to carry a load in the z-direction (Shen and Nutt 2003; Vaikhanski and Nutt 2003). Foam-LN displayed the highest stiffness index. In this case, lignin, as a binding agent, may have improved adhesion between the dispersed fibers and the continuous MC matrix. The effect is similar to the case reported by Xu et al. (2022) for a biocomposite made of CNF containing LN, in which the LN increased mechanical performance.

Compared to other biobased foams, our foams exhibited mechanical performance similar to those prepared with nanocellulose (Cervin et al. 2016; Sehaqui et al. 2010). For example, Cervin et al. (2016) reported a lightweight foam made of CNF with Young's modulus of 0.2 MPa and $\rho = 13$ kg/m^3. In the y-direction, even our reference foam (Foam-MC) exhibited a superior stiffness index. Our technology demonstrates versatility, as we could add different materials to our reference foam. Both CF and LN increased mechanical performance in the y-direction. However, the z-direction of the foam still requires tuning.

Antimicrobial and antifungal assays

All foams showed antibacterial effects (the *OD* of the foams was lower than the control) against *E. coli*. Foam-MC was the sample that performed best against bacteria. Comparable antibacterial properties were reported by Guibal et al. (2013) for a chitosan/cellulose foam tested against *E. coli*. However, by observing Foam-CF in Fig. 9, the presence of CF in the foams reduced their inhibition of bacterial growth because *ΔOD* of Foam-CF and Foam-LN was lower than for Foam-MC. On the other hand, LN appeared to protect CF from *E. coli* since Foam-LN *OD* is higher than Foam-CF. Ottenhall et al. (2018) reported that CF reduced the inhibition of bacterial growth against *E. coli* because CF can provide nutrients to *E. coli* (Ottenhall et al. 2018). On the other hand, against yeast, only Foam-CF and Foam-LN showed antifungal activity. More studies are required to elucidate the inhibition mechanisms.

Conclusions

This article presented biobased foams inspired by the main constituents of wood: cellulose and lignin. We showed that our preparation method can incorporate different additives into the foams, enhancing mechanical performance and rheology. Although our foams used macroscopic cellulose fibers, their stiffness indices in the y-direction were higher than those of typical nanocellulose foams. In terms of mechanical anisotropy, the addition of cellulose fibers and lignin to our methylcellulose foam increased the stiffness in the y-direction by a factor of three and the energy absorption in the z-direction. Furthermore, all foams showed a modest antibacterial effect against *E. coli*, without the addition of heavy metals or special surfactants. We believe that such biobased foams will have potential applications in packaging by exploiting different materials which can be foamed together with methylcellulose to tailor functionalities. In the future, it would be relevant to assess the effect of different lignin concentrations on the foam properties to optimize them for potential packaging applications.

Acknowledgements M.A., L.J., J.K., T.M. and A.P. acknowledge support from FinnCERES flagship (151830423) and Business Finland (211835). L.V. acknowledges funding from

the Vilho, Yrjö, and Kalle Väisälä Foundation via personal grants.

Author contributions Conceptualization: All the authors contributed to conceptualization. Experiments: I.MV., S.C., and Y.Z., performed the experiments. Software: I.MV. and S.C. processed the data. Formal analysis: I.MV., S.C., and T.M. contributed to the analysis. Writing draft: I.MV. wrote the original draft. Revising draft: All the author revised the manuscript. Supervision: J.K. and M.A. supervised the work. Funding: L.J., J.K., L.V., and M.A. acquired the funding for the work.

Funding Open Access funding provided by Aalto University. This work was supported by FinnCERES flagship (151830423) and Business Finland (211835).

Availability of data and materials Data is available upon request.

Declarations

Conflict of interest The authors declare that they have no conflict of interest.

Ethical approval Not applicable.

Consent to participate Not applicable.

Consent for publication The authors gave their consent for publication.

References

Alam P (2015) Biomimetic composite materials inspired by wood. In: Ansell MP (ed) Wood composites. Woodhead Publishing, pp 357–394. https://doi.org/10.1016/B978-1-78242-454-3.00014-7

Andrade A, Henríquez-Gallegos S, Albornoz-Palma G, Pereira M (2021) Effect of the chemical and structural characteristics of pulps of Eucalyptus and Pinus on the deconstruction of the cell wall during the production of cellulose nanofibrils. Cellulose 28(9):5387–5399. https://doi.org/10.1007/s10570-021-03848-0

Arvidson SA, Lott JR, Mcallister JW, Zhang J, Bates FS, Lodge TP, Sammler RL, Li Y, Brackhagen M (2013) Interplay of phase separation and thermoreversible gelation in aqueous methylcellulose solutions. Macromolecules 46(1):300–309. https://doi.org/10.1021/ma3019359

Ashby MF, Medalist RFM (1983) The mechanical properties of cellular solids. Metall Trans A 14(9):1755–1769. https://doi.org/10.1007/bf02645546

Balakshin MY, Capanema EA, Sulaeva I, Schlee P, Huang Z, Feng M, Borghei M, Rojas OJ, Potthast A, Rosenau T et al (2021) New opportunities in the valorization of technical lignins. Chemsuschem 14(4):1016–1036. https://doi.org/10.1002/cssc.202002553

Boeriu CG, Bravo D, Gosselink RJ, van Dam JE (2004) Characterisation of structure-dependent functional properties of lignin with infrared spectroscopy. Ind Crops Prod 20(2):205–218. https://doi.org/10.1016/j.indcrop.2004.04.022, 6th International Lignin Institute conference

Budtova T, Navard P (2016) Cellulose in NaOH-water based solvents: a review. Cellulose 23(1):5–55. https://doi.org/10.1007/s10570-015-0779-8

Cervin NT, Johansson E, Larsson PA, Wågberg L (2016) Strong, water-durable, and wet-resilient cellulose nanofibril-stabilized foams from oven drying. ACS Appl Mater Interfaces 8(18):11682–11689. https://doi.org/10.1021/acsami.6b00924

Chandler D (2005) Interfaces and the driving force of hydrophobic assembly. Nature 437(7059):640–647. https://doi.org/10.1038/nature04162

Coughlin ML, Liberman L, Ertem SP, Edmund J, Bates FS, Lodge TP (2021) Methyl cellulose solutions and gels: fibril formation and gelation properties. Prog Polym Sci 112:101324. https://doi.org/10.1016/j.progpolymsci.2020.101324

Derkacheva O, Sukhov D (2008) Investigation of lignins by FTIR spectroscopy. Macromol Symp 265(1):61–68. https://doi.org/10.1002/masy.200850507

Faix O (1991) Classification of lignins from different botanical origins by FT-IR spectroscopy. Holzforschung 45(s1):21–28. https://doi.org/10.1515/hfsg.1991.45.s1.21

Ferreira ES, Cranston ED, Rezende CA (2020) Naturally hydrophobic foams from lignocellulosic fibers prepared by oven-drying. ACS Sustain Chem Eng 8(22):8267–8278. https://doi.org/10.1021/acssuschemeng.0c01480

Ferreira ES, Rezende CA, Cranston ED (2021) Fundamentals of cellulose lightweight materials: bio-based assemblies with tailored properties. Green Chem 23(10):3542–3568. https://doi.org/10.1039/d1gc00326g

Gavin C, Verbeek CJR, Lay MC (2018) Morphology and compressive behaviour of foams produced from thermoplastic protein. J Mater Sci 53(22):15703–15716. https://doi.org/10.1007/s10853-018-2714-5

Ghanbari A, Mousavi Z, Heuzey M, Patience GS, Carreau PJ (2020) Experimental methods in chemical engineering: rheometry. Can J Chem Eng 98(7):1456–1470. https://doi.org/10.1002/cjce.23749

Gibson LJ (2012) The hierarchical structure and mechanics of plant materials. J R Soc Interface 9(76):2749–2766. https://doi.org/10.1098/rsif.2012.0341

Gibson LJ, Ashby MF (1997) Cellular solids: structure and properties, 2nd edn. Cambridge solid state science series. Cambridge University Press, Cambridge. https://doi.org/10.1017/CBO9781139878326

Guibal E, Cambe S, Bayle S, Taulemesse JM, Vincent T (2013) Silver/chitosan/cellulose fibers foam composites: from synthesis to antibacterial properties. J Colloid Interface Sci 393:411–420. https://doi.org/10.1016/j.jcis.2012.10.057

Hjelt T, Ketoja JA, Kiiskinen H, Koponen AI, Pääkkönen E (2021) Foam forming of fiber products: a review. J Dispers Sci Technol. https://doi.org/10.1080/01932691.2020.1869035

Jiang Z, Ngai T (2022) Recent advances in chemically modified cellulose and its derivatives for food packaging applications: a review. Polymers 14(8):1533. https://doi.org/10.3390/polym14081533

Kaliyan N, Morey RV (2010) Natural binders and solid bridge type binding mechanisms in briquettes and pellets made from corn stover and switchgrass. Biores Technol 101(3):1082–1090. https://doi.org/10.1016/j.biortech.2009.08.064

Kerche EF, Bock DN, De Avila Delucis R, Magalhães WLE, Amico SC (2021) Micro fibrillated cellulose reinforced bio-based rigid high-density polyurethane foams. Cellulose 28(7):4313–4326. https://doi.org/10.1007/s10570-021-03801-1

Klemm D, Heublein B, Fink HP, Bohn A (2005) Cellulose: fascinating biopolymer and sustainable raw material. Angew Chem Int Ed 44(22):3358–3393. https://doi.org/10.1002/anie.200460587

Korhonen O, Budtova T (2019) Gelation of cellulose-NaOH solutions in the presence of cellulose fibers. Carbohyd Polym 224:115152. https://doi.org/10.1016/j.carbpol.2019.115152

Larkin P (2018) Infrared and Raman spectroscopy: principles and spectral interpretation. Elsevier. https://doi.org/10.1016/C2015-0-00806-1

Li T, Chen C, Brozena AH, Zhu JY, Xu L, Driemeier C, Dai J, Rojas OJ, Isogai A, Wågberg L et al (2021) Developing fibrillated cellulose as a sustainable technological material. Nature 590(7844):47–56. https://doi.org/10.1038/s41586-020-03167-7

Lott JR, Mcallister JW, Arvidson SA, Bates FS, Lodge TP (2013) Fibrillar structure of methylcellulose hydrogels. Biomacromol 14(8):2484–2488. https://doi.org/10.1021/bm400694r

Ma Y, Asaadi S, Johansson LS, Ahvenainen P, Reza M, Alekhina M, Rautkari L, Michud A, Hauru L, Hummel M et al (2015) High-strength composite fibers from cellulose-lignin blends regenerated from ionic liquid solution. Chemsuschem 8(23):4030–4039. https://doi.org/10.1002/cssc.201501094

Ma C, Kim TH, Liu K, Ma MG, Choi SE, Si C (2021) Multifunctional lignin-based composite materials for emerging applications. Front Bioeng Biotechnol. https://doi.org/10.3389/fbioe.2021.708976

Miranda-Valdez IY (2022) Non-structural applications of Ioncell®carbon fibers. Master's thesis, Aalto University. School of Chemical Engineering. http://urn.fi/URN:NBN:fi:aalto-202206194011

Miranda-Valdez IY, Viitanen L, Intyre JM, Puisto A, Koivisto J, Alava M (2022) Predicting effect of fibers on thermal gelation of methylcellulose using Bayesian optimization. Carbohyd Polym 298:119921. https://doi.org/10.1016/j.carbpol.2022.119921

Mort R, Vorst K, Curtzwiler G, Jiang S (2021) Biobased foams for thermal insulation: material selection, processing, modelling, and performance. RSC Adv 11(8):4375–4394. https://doi.org/10.1039/d0ra09287h

Nanou P, Huijgen W, Carbo M, Kiel J (2018) The role of lignin in the densification of torrefied wood in relation to the final product properties. Biomass Bioenerg 111:248–262. https://doi.org/10.1016/j.biombioe.2017.05.005

Ottenhall A, Seppänen T, Ek M (2018) Water-stable cellulose fiber foam with antimicrobial properties for bio based low-density materials. Cellulose 25(4):2599–2613. https://doi.org/10.1007/s10570-018-1738-y

Reichler M, Rabensteiner S, Törnblom L, Coffeng S, Viitanen L, Jannuzzi L, Mäkinen T, Mac Intyre JR, Koivisto J, Puisto A et al (2021) Scalable method for bio-based solid foams that mimic wood. Sci Rep. https://doi.org/10.1038/s41598-021-03764-0

Rhim JW, Park HM, Ha CS (2013) Bio-nanocomposites for food packaging applications. Prog Polym Sci 38(10):1629–1652. https://doi.org/10.1016/j.progpolymsci.2013.05.008. (**progress in Bionanocomposites: from green plastics to biomedical applications**)

Sehaqui H, Salajková M, Zhou Q, Berglund LA (2010) Mechanical performance tailoring of tough ultra-high porosity foams prepared from cellulose I nanofiber suspensions. Soft Matter 6(8):1824. https://doi.org/10.1039/b927505c

Shen H, Nutt S (2003) Mechanical characterization of short fiber reinforced phenolic foam. Compos A Appl Sci Manuf 34(9):899–906. https://doi.org/10.1016/S1359-835X(03)00136-2

Tejado A, Chen WC, Alam MN, Van De Ven TGM (2014) Superhydrophobic foam-like cellulose made of hydrophobized cellulose fibres. Cellulose. https://doi.org/10.1007/s10570-014-0247-x

Trogen M, Le ND, Sawada D, Guizani C, Lourençon TV, Pitkänen L, Sixta H, Shah R, O'Neill H, Balakshin M et al (2021) Cellulose-lignin composite fibres as precursors for carbon fibres. Part 1—manufacturing and properties of precursor fibres. Carbohyd Polym 252:117133. https://doi.org/10.1016/j.carbpol.2020.117133

Vaikhanski L, Nutt SR (2003) Fiber-reinforced composite foam from expandable PVC microspheres. Compos A Appl Sci Manuf 34(12):1245–1253. https://doi.org/10.1016/S1359-835X(03)00255-0

Vuoriluoto M, Hokkanen A, Mäkelä T, Harlin A, Orelma H (2022) Optical properties of an organic-inorganic hybrid film made of regenerated cellulose doped with light-scattering TiO_2 particles. Opt Mater 123:111882. https://doi.org/10.1016/j.optmat.2021.111882

Xu K, Li Q, Xie L, Shi Z, Su G, Harper D, Tang Z, Zhou J, Du G, Wang S (2022) Novel flexible, strong, thermal-stable, and high-barrier switchgrass-based lignin-containing cellulose nanofibrils/chitosan biocomposites for food packaging. Ind Crops Prod 179:114661. https://doi.org/10.1016/j.indcrop.2022.114661

Yang C, Tartaglino U, Persson B (2006) Influence of surface roughness on superhydrophobicity. Phys Rev Lett 97(11):116103. https://doi.org/10.1103/PhysRevLett.97.116103

Yang H, Yan R, Chen H, Lee DH, Zheng C (2007) Characteristics of hemicellulose, cellulose and lignin pyrolysis. Fuel 86(12):1781–1788. https://doi.org/10.1016/j.fuel.2006.12.013

Yu J, Paterson N, Blamey J, Millan M (2017) Cellulose, xylan and lignin interactions during pyrolysis of lignocellulosic biomass. Fuel 191:140–149. https://doi.org/10.1016/j.fuel.2016.11.057